Blink: Detecting, Storing and Analysing Eye Blinks

Aayush Chadha

Supervised by: **Professor Thomas Thomson**

Final year project report submitted for the degree of **BSc. (Hons) Artificial Intelligence**

School of Computer Science

Faculty of Science and Engineering, University of Manchester

April 2019

Acknowledgements

This project wouldn't have been possible without the extensive help of several people. First and foremost, I owe a huge debt of gratitude to my supervisor, Professor Thomas Thomson, for letting me run free with an ambitious idea and for being an exceptional source of advice throughout the year. In a similar vein, I would also like to thank Professor Simon Harper for his support to get the project off the ground.

A huge debt of gratitude is also owed to Dr. Gregory Auton and Dr. Alexander Lincoln, who were more than generous with their time when it came to explaining, demonstrating and helping brainstorm many of the experimental procedures that underpin the work done here and without whom, I would have not achieved any of the results I did.

Amongst my friends, I would specifically like to mention Surjo Dutta, Abhinav Rao and Rifad Lafir for being patient sounding boards for ideas and occasionally, sources of insight and knowledge. I would also like to thank Tüge Neumann and Raj Dholakia for parting with their actuators at a crucial juncture for this project. In addition to them, there were a lot of other friends who, willingly or unwillingly, indulged my ramblings about this project for a year and I would like to thank them all as well!

Finally, I would like to express my thanks to my family, who were very patient when it came to continuous hangout calls about failed experiments and were a constant source of support and encouragement through the trials of research.

Abstract

In a world consisting of a rapidly ageing population, health monitoring and healthcare delivery are becoming important concerns. The benefits of early diagnosis and intervention with regards to age related health issues are key to helping people live healthy and productive lives. Two of the most significant age-related disorders are Parkinson's Disease and Alzheimer's, both of which are difficult to diagnose and monitor on a long term basis. This multidisciplinary project seeks to establish a first step towards better diagnosis and monitoring by utilising 2D materials, such as graphene, to construct wearable sensors that can be linked to low cost micro-controllers for continuous and unobtrusive monitoring. In doing so, it unites the fields of neuroscience, computer science and 2D materials. The project first establishes the requirements for the overarching work it intends to complete and then surveys existing work on eye blinking, Parkinson's Disease and applications of 2D materials for human motion monitoring. It then successfully goes on to build an end to end system that can detect synthetic eye blinks, analyse the raw data and present it in an intuitive manner for physicians to use. These results provide a successful proof of concept for the application of 2D materials towards monitoring neurodegenerative diseases. Lastly, it suggests promising paths to take to make such devices more effective and clinically acceptable.

Table of Contents

List of Figures

1. Introduction

The aim of this interdisciplinary project is to build an end to end system that detects eye blinks in a human subject and transmits this data across a wired connection onto a micro-controller which is able to store it. The stored data is then analysed to identify trends that could indicate the presence of neurodegenerative disorders, such as Parkinson's Disease (PD). Achieving the project's goals would represent the first step in the construction of a system that can monitor eye blinking outside of clinical settings. Long term studies, such as those that would be enabled by the system proposed and prototyped below, can then be conducted to understand the effects of the disease on eye blinking outside of clinical settings, something that hasn't been possible so far due to the lack of appropriate equipment. Additionally, current studies have focussed on assessing the impact of the disease on motor function at fixed time intervals. This represents a drawback in their evaluation since the symptoms of Parkinson's are asymmetric, i.e, they occur sporadically with no precise pattern. The proposed device gets around this limitation by providing a continuous stream of data that can be vital in the creation of better intervention strategies.

However, to build such a device, one must ensure that sensing is carried out unobtrusively. This is important since an obtrusive sensing technology can easily impact the behaviour of the subject. Furthermore, such a device must be sensitive enough to pick up faint strains on a consistent basis. To achieve these objectives, a wide variety of organic and inorganic materials have been studied, which, given their excellent optical and electrical properties lend itself quite well to such

applications. Examples of such materials include 2D materials like graphene, which has been extensively studied for its applications in the field of biomedical sensing amongst other things. Armed with this knowledge, the following project aims emerge:

- Examine the applicability of graphene for human motion monitoring.
- Integrate sensors with a low cost system capable of measuring electrical changes and storing the data.
- Automate the process of data analysis.
- Allow end to end integration of the above components to provide physicians with an additional tool to monitor the disease effectively.

The following sections will address the above aims. **Chapter 2. Background** starts off with building the biological basis for the relation between eye blinks and Parkinson's Disease. It then expounds the properties of 2D materials and graphene in particular to justify its suitability for this project. Finally, it surveys the breadth of existing work done on eye blink detection, Parkinson's Disease and the use of 2D materials for human motion monitoring. **Chapter 3. System Design** discusses the proposed pipeline utilised by this project and the various components that constitute it. This chapter also discusses some alternative choices that could be made at various stages of the project and provides arguments in support of the choices made. **Chapter 4. Implementation** shows how each of the above aims were addressed by creating a tangible, end to end system. It also provides a more in-depth discussion of the implementation details and the various stages of iteration. **Chapter 5. Testing and Results** provides information on testing the prototype and shows the results that were obtained, which include the detection of synthetic eye blinks and automated analysis of the raw electrical measurement data. Finally, **Chapter 6. Conclusion and Reflection** assesses the success of the work undertaken, reflects on the choices made in terms of planning the project and mentions the future directions that this project could take.

2. Background

This section seeks to build a biological basis for the relation between eye blinking and Parkinon's Disease, look at properties of 2D materials and highlight the nature of work already undertaken in order to detect blinks and carry out strain sensing for biomedical applications. Furthermore, it attempts to provide some context to the design decisions made in the development of the sensor for this project.

2.1 Eye blinking

Eye blinking in humans is the function of 3 primary muscles, the orbicularis oculi (OO), levator palpebrae superioris and the superior tarsal muscle [1]. For the rest of this report, we are going to concern ourselves with the movement characteristics of the OO muscle.

The OO muscle is located in the eyelids and is arranged in a concentric band in each one of them. It's the contraction of these muscles that allows for the closing of eyelids and carrying out the blink movement. [2].

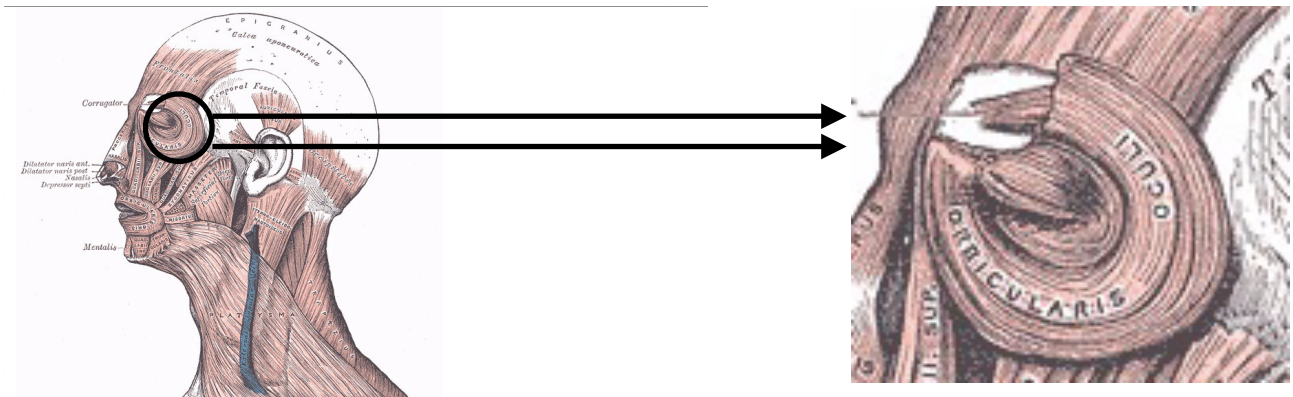

Head Face and Neck Muscles, Epicranius, Galea aponeurotica, Frontalis, Temporal Fascia, Auricularis Superior, Auricularis Anterior, Auricularis Posterior, Occipitalis, Sternocleidomastoid, Platysma, Trapezius, Orbicularis Oculi, Corrugator, Procerus Nasalis, Dilatator Naris Anterior, Dilatator Naris Posterior, Depressor Septi, Mentalis, Orbicularis Oris, Masseter, Zygomaticus, Risorius. Contributed by Gray's Anatomy Plates

Figure 2.1: Head and Neck Anatomy (Taken from - Tong 2018) [2]

A blink can be classified into three broad categories. These categories are voluntary, involuntary/ spontaneous and reflex. A voluntary blink is best defined as actively engaging the orbicularis oculi muscle to close the eyelid. In contrast, the blink reflex is an autonomous reaction generated in response to an external stimulus, such as the threat of danger from an approaching object or the irritation of the cornea amongst other things.

Spontaneous blinks occur in the absence of any conscious effort or external stimulus. In patients suffering from progressive neurodegenerative diseases, such as Parkinson's disease, some of the above blink patterns mentioned have been found to differ from healthy subjects [3].

2.2 Parkinson's Disease

Parkinson's Disease is a progressive neurodegenerative disorder characterised by symptoms such as shakiness, tremor, slowed down movements and a loss of balance. These symptoms are collectively referred to as Parkinsonism and can be caused by a variety of diseases. Parkinsonism caused by Parkinson's Disease (PD) is called primary Parkinsonism.

The underlying cause of Parkinson's Disease is still subject to speculation and experimental study [4]. However, it is known that Parkinson's results in a loss of dopamine-producing neurones in a region of the brain called substantia nigra (SN). The loss of these neurones affects the ability of the motor cortex to undertake and regulate movement of the muscles, thereby leading to the movement symptoms highlighted above and hence affecting the rate of blinking. The exact mechanism of how this occurs is described below.

2.2.1 Pathophysiology of Parkinson's Disease

Movement control of the human body can be divided into two tasks. The first task is the ability to undertake required movements and the second task is to prevent unwanted movements. These tasks are coordinated in a region of the brain called the basal ganglia [5].

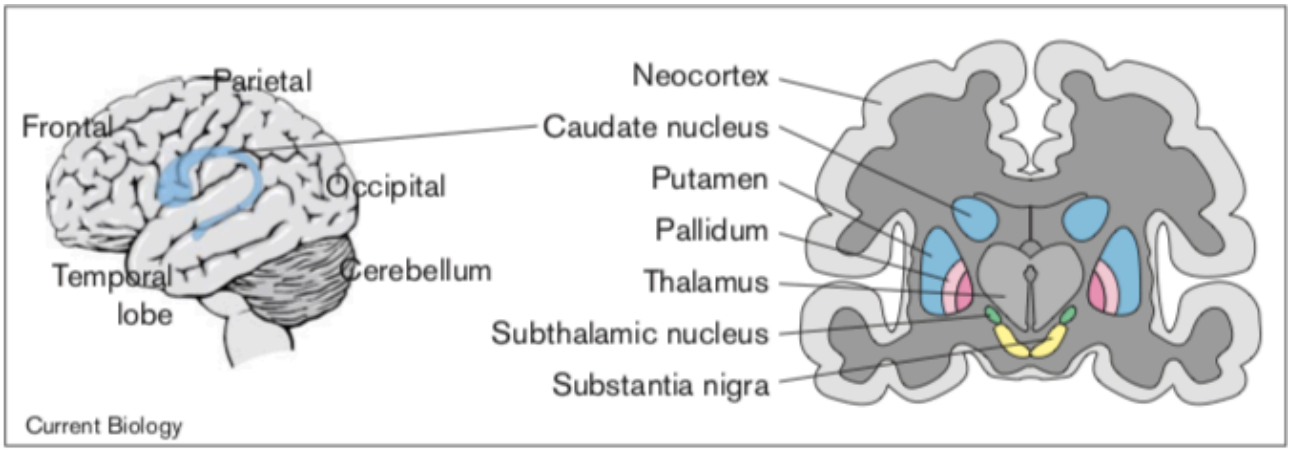

Figure 2.2: Brain Cross-Section Showing the Basal Ganglia (Taken from - Graybiel 2000) [6]

The basal ganglia has two pathways that allow the aforementioned tasks to occur, the direct and the indirect pathway. These pathways are collections of nuclei that communicate with each other through the use of neurotransmitters. The effect of these neurotransmitters is either inhibitory or excitatory. Both these pathways are regulated by the substantia nigra, which contains dopamine neurones.

The direct pathway, which is responsible for carrying out movement, is able to perform its task by reducing inhibition of the thalamus, which in turn allows the motor cortex to be excited and carry

out movement. All of this is allowed to happen by the substantia nigra, which synapses with the striatum's D1 receptors. The D1 receptors end up activating the striatum's inhibitory neurones and these inhibitory neurones in turn transmit an inhibitory neurotransmitter called GABA to inhibit the globus pallidus. The globus pallidus, which until now has been inhibiting the thalamus, is inhibited itself. The thalamus is hence able to excite the motor cortex, allowing movement to occur.

The indirect pathway prevents unwanted movement from occurring. To do so, the substantia nigra must have the opposite effect on the striatum so that the globus pallidus is more active than usual and therefore the thalamus is inhibited. It does this by transmitting dopamine that binds with the D2 receptors in the striatum. This results in the inhibition of the striatum's inhibitory neurones. Consequentially, the globus pallidus is no longer inhibited and is able to inhibit the thalamus much more and subsequently, the motor cortex, preventing movement from occurring.

The loss of these dopamine producing neurones in the substantia nigra causes Parkinson's and Parkinson's like diseases by jeopardising the functionality of the direct and the indirect pathway. [7]

2.3 2D Materials

2D materials are a class of crystalline materials which are defined by their single or few atomic layers property. The number of atomic layers and their crystal structures can cause the same chemical compound to exhibit different properties as the layers and structures are varied [8]. One of the most famous and extensively studied 2D material is graphene, which is a single layer arrangement of carbon atoms.

Following the isolation and examination of few-layer graphene at the University of Manchester in 2004 [9], there has been a spur of activity identifying the uses of graphene. Its applications span several industries, including biomedical sensing. The suitability of graphene for such applications is explained below.

2.3.1 Properties of Graphene

Graphene's structure is defined by a single layer, benzene-ring structure of carbon atoms. [9] Inspite of its thickness (<3nm), graphene and related materials remain stable under ambient conditions while displaying strong conductivity and flexibility. The excellent electrical properties of graphene are a result of the following characteristics of its structure:

- It doesn't contain a band gap, which allows electrons to move freely between the valence and conduction bands. It's described as a zero-bandgap semiconducting material.
- The covalent bonds between carbon atoms contain a free 4th electron that can move freely between the lattice. This leads to a high carrier density.
- It has high carrier mobilities, exceeding $15000 cm^2/Vs$, even under ambient conditions. [10] Silicon, in comparison, has an electron mobility of $\leq 1400 cm^2/Vs$ and a hole mobility of $\leq 450 cm^2/Vs$ [11]. Then again, silicon also has a band gap.
- It can support current densities 100 times higher than those supported by copper. [12]

In addition to these, graphene is also opaque [13], making it well suited for unobtrusive sensing applications. Moreover, a Young's modulus of 1TPa [14] allows it to maintain its conductance even under significant strain. Finally, a gauge factor that can potentially reach 10^6 [15] through suitable fabrication techniques makes graphene an excellent candidate for highly sensitive strain sensing.

2.4 Blink Detection

The task of detecting blinks isn't exclusive to the domain of neurodegenerative diseases. Eye blinks can serve as useful markers in a variety of domains, from facial rehabilitation [16], driver fatigue sensing [17, 18, 19, 20] to dry eyes sensing [21]. All these sources represent different approaches to solving the same problem, each with its own set of benefits and drawbacks for continuous blink detection.

2.4.1 Blink Detection Using Camera Based Techniques

As cameras become smaller and more pervasive, they represent a natural choice for a wide variety of monitoring applications. Smith et al. (2000) [17] showed how it is possible to extract facial feature information from a camera mounted on a driver's dashboard. All of this information was retrieved through the analysis of 320x240 size images from a 30fps video and the system was tested with two drivers under different conditions.

Likewise, Fan et. al (2007) [18] attempted to classify yawning based on facial feature detection using Linear Discriminant Analysis (LDA). Again, the data was collected through a camera and fed through an image processing pipeline that extracted feature vectors for the LDA algorithm to use.

The critical component underlying these and related approaches is the need for several components and extensive analysis before desirable results can be seen.

2.4.2 Blink Detecting Using Infrared Based Techniques

Frigerio et al. (2014) [16] demonstrated the construction of a wearable device that assists with the rehabilitation of patients suffering from facial paralysis. The problem they sought to solve was to prevent damage to the perpetually open eye which was exposed to debris and chronic irritation due to the paralysis of the orbicularis oculi muscle. Their method made use of an infrared based device which detected blinks on one side of the eye and simultaneously triggers a blink on the paralysed side. It also sought to provide an alternative to contact based approaches that relied on electromyographic (EMG) recording of the orbicularis oculi muscle.

While effective in detecting blinks and much less inconspicuous than camera based approaches, the approach did require suitable adjustment of the infrared emitter/receiver pair to account for varying facial structures. Another drawback of the presented approach was its sensitivity to detect blink events when the gaze was lowered, leading to natural interruption of the infrared beam by the upper eyelid. Similar work was undertaken by Dementyev et al. (2017) [21] with the aim to alleviate computer vision syndrome.

Again, it proved to be a successful approach but one that suffers from the same drawbacks as the previous work and requiring further investigation in longitudinal scenarios, to overcome issues such as the shifting of the sensors and the exposure to direct sunlight which could influence the infrared receiver.

2.5 Effects of Parkinson's Disease on Blinking

The effect neurodegenerative diseases on the blink reflex has been known since the 1960s, when Rushworth (1962) [22] showed how the blink reflex varies with patients presenting Parkinson's like symptoms. Kimura (1973) [23] provided evidence in support of the hypothesis which suggested that the blink reflex was changed in Parkinson's patients because of the effects of the diseases on the interneurons, a finding that is consistent with our current understanding of the direct and indirect pathways underlying motor control.

Basso et. al (1993) [24] provided an explanation for the hyper excitable reflex blinks in PD patients by providing data that supported ideas related to the changes in the inhibitory effect of the structures present in the basal ganglia. Karson (1983) [25] demonstrated the existence of a possible relationship between dopaminergic activity and eye blinking, not only in patients with Parkinson's but also Schizophrenia.

In more recent times, the work of Agostino et al. (2008) [3] investigated the effects of medication on blink kinematics and suggested differences in pathophysiological mechanisms underlying the three different types of blinking. It also concluded that the blink rates are abnormal in patients with Parkinson's Disease. These findings and other similar works were comprehensively summarised by Jongkees et al. (2016) [26] which established that eye blink rate can be used as an informative predictor of dopaminergic activity.

2.6 Strain Sensing

2.6.1 Strain Sensing Using the Piezoelectric Effect

The piezoelectric effect, where an electric charge accumulates in a structure under mechanical stress provides the foundation for several strain sensing applications. With recent advances in material sciences and fabrication techniques, it is now possible to manufacture piezoelectric devices that are thin, flexible and for biomedical applications, biocompatible.

One of the most extensively studied piezoelectric material for biomedical applications is Zinc Oxide (ZnO) [27]. Lee et al. (2012) [28] demonstrated the construction of a piezoelectric sensor using nano wires made out of ZnO that can be used to detect blinks through the generation of a 0.2V voltage and a 2nA current. The device used an aluminium foil of 18μm as the substrate and the electrode. The key contribution of their approach was the fact that they created a self powered device not requiring an external power source. Applications of piezoelectric materials in the development of self-powered miniature sensors remains an interesting approach.

2.6.2 Strain Sensing Using 2D Materials

Alternatively, 2D materials represent another exciting frontier for strain sensing applications given their unique electromechanical and optical properties. These properties lend itself well to strain sensing since it makes for unobtrusive sensors that are biocompatible, sensitive and near invisible when applied to the skin. Graphene is an excellent example of a material that falls within this category and it has already been extensively used in skin based strain sensing applications as depicted in the works of Xiao et al. (2012) [15] and Wang et al. (2014) [29]. In fact, the latter's work involved building a sensor that was able to pick up eye blinks on a digital source meter (Keithley 2602 and Keithley 4200-SCS). Their results, which are reproduced below prove

extremely useful in guiding the choice of a micro controller as well since the relative change in resistance can give us information about the desired voltage resolution. This has been discussed further in **Section 3.4.1**.

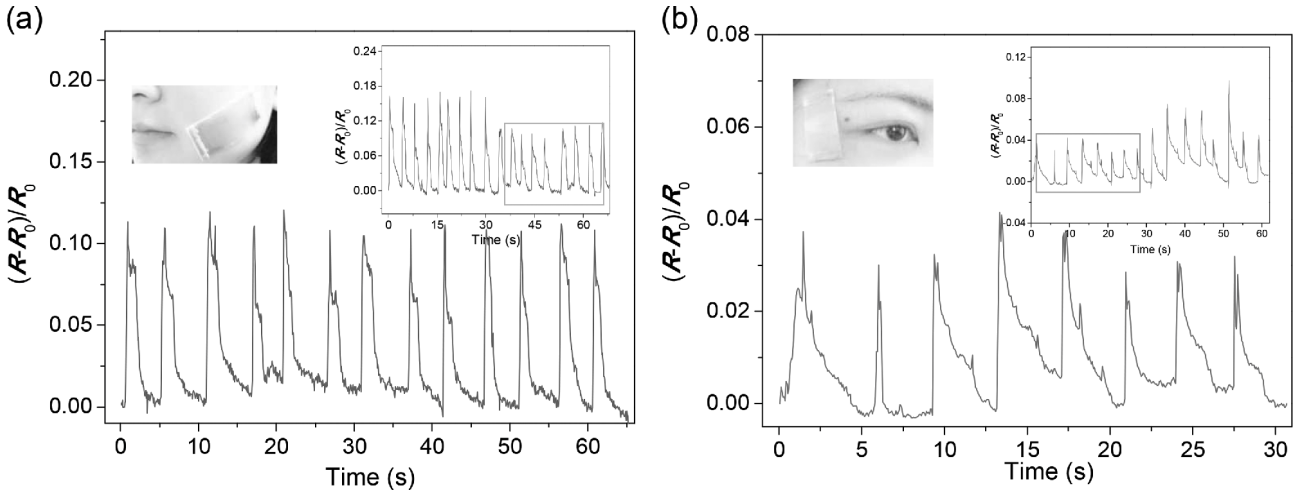

Fig 2.3: Measured changes in resistance for eye blinks (Taken from - Wang et. al 2014) [29]

3. System Design

The previous section has served to establish a strong foundation for the necessity of such a device and has surveyed various approaches and their drawbacks with regards to blink monitoring and strain sensing. We can now adequately define the requirements of a pipeline and it's constituent components that accomplish the goals of blink sensing and the analysis of that information.

3.1 Blink Pipeline Requirements

Following our previous discussions, the following requirements emerge:

- The device must be worn for long durations of time without causing pain or discomfort to the user.

- The sensor itself should be sensitive enough to pick small strains.
- Repeated strain cycles shouldn't damage the sensor extensively.
- The data should be collected on a micro controller that is able to store data to avoid transmission over Bluetooth or WiFi networks, since that increases complexity for the user.
- The micro controller should be sensitive enough to detect small changes in resistance (1-2%).
- The sensing circuit should make use of as few components as possible to allow for easy integration into a completely wearable system.
- The physicians should be able to get the results of the data analysis with the least amount of technical friction.

Since the sensors are finally attached to the skin, there must also exist a repeatable testing procedure to ensure that the sensors work as intended.

3.2 Proposed Pipeline Design

Given those requirements, the resultant pipeline can be represented as follows:

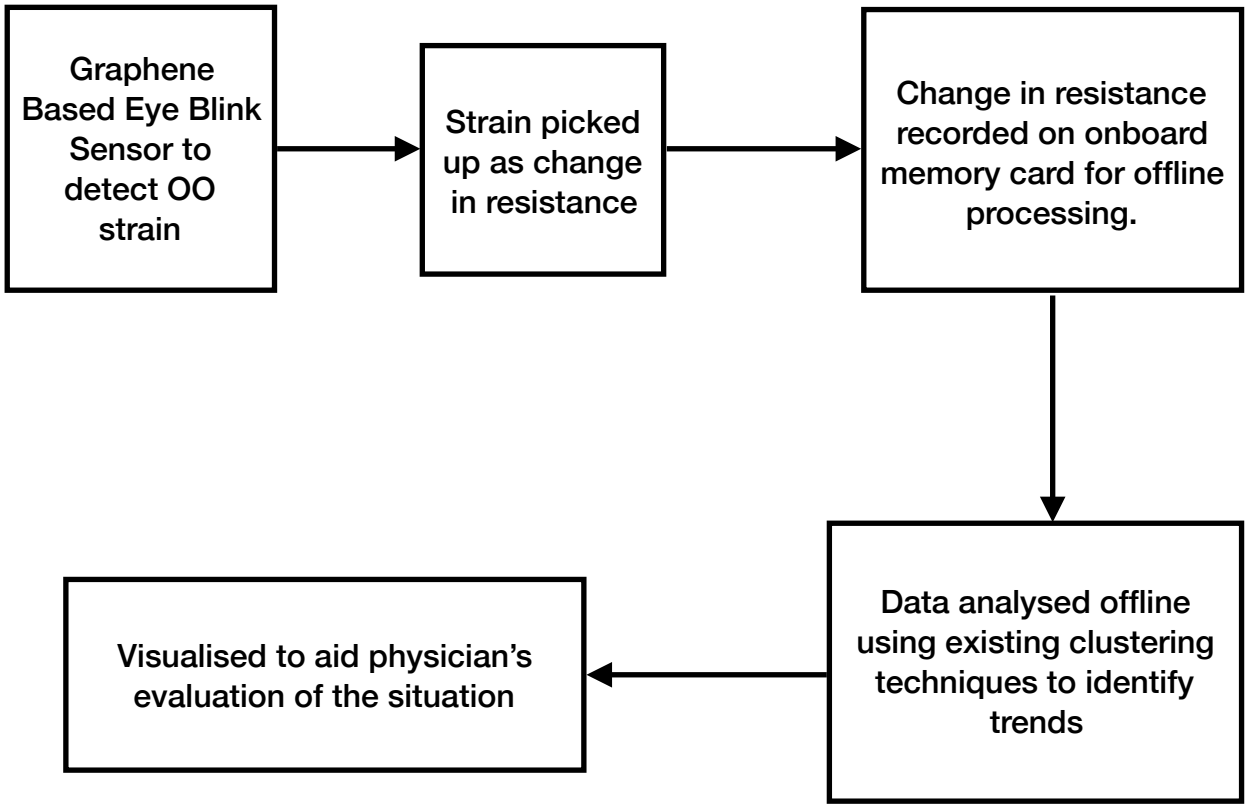

Fig 3.1: Blink Monitoring Pipeline

Several choices exist at various stages of the pipeline that would serve the defined purpose equally well. The next section presents an overview of the choices made at each stage.

3.3 Building the sensor

3.3.1 Choosing the sensing element

Several possible materials can be used as the sensing material. To make a good strain gauge, nonetheless, one requires a material that isn't constrained by the direction of the strain and has high resolution. The requirement of these properties excludes traditional strain measuring devices, such as those made of out of semiconducting materials.

Carbon based nano-materials represent a good choice in terms of sensing material. Apart from graphene, another possibility arises in the use of Carbon Nanotubes (CNTs) for strain sensing [30, 31]. Graphene and CNTs have similar properties and respond to strain in a predictable manner. Despite that, there are differences that emerge when large scale production has to be considered. CNTs are hard to manufacture in their one dimensional form which underpins many applications. This prevents them from being built at scale for complex sensing applications. Graphene on the other hand is highly amenable to micro-fabrication processes, an example of which is mentioned in our fabrication process as well. The other difference lies in the relatively defect free production of graphene, whereas CNTs on the other hand contain impurities that alter the response characteristics and make it hard to reproduce results [32]. Given these factors, graphene represented a choice that didn't involve an extensive fabrication process, produced defect-free samples and owing to the large interest in them, also had suitable literature to address a huge majority of challenges. This meant we could avoid dealing with challenges that would eat into the development time of the project.

Ultimately, it was an ideal choice combining rapid development, biocompatibility and sensing ability.

3.3.2 Choosing substrates

While we have a sensible material to pick up the strain, the thickness of graphene is only 0.345nm [33]. This thickness prevents the sheet from being useful on its own without any flexible substrate to support it. The natural choice for a flexible substrate is polydimethylsiloxane (PDMS), which is a silicone based organic polymer. The main benefits of PDMS are its biocompatibility and a Young's modulus of 360-870KPa [34]. It can also be used to manufacture thin films in the 50-100µm range, which is well suited for our application. While PDMS is non irritating when in contact with the skin [34], it isn't naturally adhesive. To counteract that, a thin enough adhesive layer that would allow us to attach our graphene + PDMS stack to the skin had to be chosen.

Medical tapes are often used for most wearable sensing applications. For this work, the following tapes were considered, all of which were provided by 3M™.

Tape Name	Adhesive Type	Conformability	Intended Usage	Thickness (mm)	Reference
2476P	Silicone	High	Wound care dressing	0.37	35
1522	Acryclic	Medium	Surgical drapes	0.16	36
2477P	Silicone Acrylate	High	Adhesion to skin	0.18	37

Figure 3.2: Comparison between adhesive materials

2476P and 2477P are the obvious candidates because of their high degree of conformability. Since we already have a 50μm thick layer of PDMS, 2477P becomes the natural choice since the overall stack thickness is kept low.

3.4 Building the electrical signal measuring unit

3.4.1 Choosing a micro controller

Before a sensible micro controller to detect blinks is chosen, it is useful to look into the typical values for the strain we seek to measure. From the discussion in **Section** Their results show that a typical eye blink leads to a 2-4% change in resistance of the sensor. Using this result, we can calculate the voltage resolution needed on our micro controller. The calculations below assume that R_0, the resistance of the graphene film at rest (unstrained) is 2kΩ (this isn't an entirely baseless assumption, several samples that we prepared had similar resistance values while at rest). A 2-3% change in resistance would imply that the resistance increases by 40-60Ω.

Using the familiar relation between voltage and resistance,

$$I = \frac{V}{R}$$

and assuming we hold voltage constant at 1V, we can find the current across the sheet under strain by:

$$I = \frac{1}{2040} \approx 490\mu A$$

The value calculated above is the minimum current value that the strained sheet approaches. By a similar calculation, we find out that when graphene is unstrained, we have a current value of $500\mu A$.

This translates to a $10\mu A$ change as the sheet is strained, at the very minimum.

Now to ascertain whether a standard micro controller can pick this strain up, we need to calculate their voltage resolutions. Since we were primarily interested in boards with space for an on-board memory card, Adafruit M0 Datalogger and Teensy 3.5/3.6 were two possible choices. Both these boards provide an onboard voltage reference of $3.3V$ [38, 39]. In addition to that, a 1.1V internal reference is available as well [40]. The Teensy features 2 analog-to-digital converters (ADC) with 13-bit resolution and 2 digital-to-analog converters (DAC) with 12-bit resolution [39]. The M0, on the other hand, has a 12-bit ADC and a single 10 bit DAC [38].

The bit resolution of the ADC means that an analog signal, such as a voltage measurement can be represented as a digital signal in one of the $2^{12}(4096)$ states. Using the standard $3.3V$ reference, we find out that to move between states, a voltage change of $0.8mV$ $(\frac{3.3}{4096})$ is required. Likewise, this step size can be made smaller if we use the onboard internal reference, which gives us a step-size of $0.2mV$.

Again, by using $V = IR$, we find out that a $10\mu A$ change is equivalent to a voltage of 20mV, which is 100 steps. Both the boards have a more than reasonable resolution to pick up the strains we intend to see. The project ended up testing both the boards, however, given M0's form factor and ease of use, it represents the slightly better choice when it comes to boards.

3.5 Automating data analysis

3.5.1 Workflow orchestration framework

An important constraint of the project was to ensure that the data collected by the sensors, which would be raw voltage readings with timestamps, could be analysed by physicians without requiring any knowledge of either programming or sensor data analysis. This overarching requirement meant that any tool used by them to retrieve results should require minimal setup, be visual, have clearly explained documentation and allow for easy updates of the underlying analysis mechanism based on feedback.

Two workflow orchestration frameworks were considered. Apache Airflow [41] and Apache Taverna [42], both open source projects supported by the Apache Foundation, had similar functionality. Airflow represents workflows as directed acyclic graphs that can be created using the Python programming language and then visualised using the user interface. While Airflow contains a huge set of features, its primary drawback is the requirement of a pre-installed Python environment for setup. In contrast to Taverna, one can't share workflows through a common portal on the internet such as myExperiment [43]. Installation of Taverna is also simpler in comparison to Airflow, since it's primarily Java based and therefore, platform agnostic.

4. Implementation

4.1 Building the sensor

Lee et al. (2010) [44] measured the gauge factor of graphene films on flexible substrates to be ~6.1 at an applied strain of 1%. This is much better than standard metal alloy based strain gauges [45].

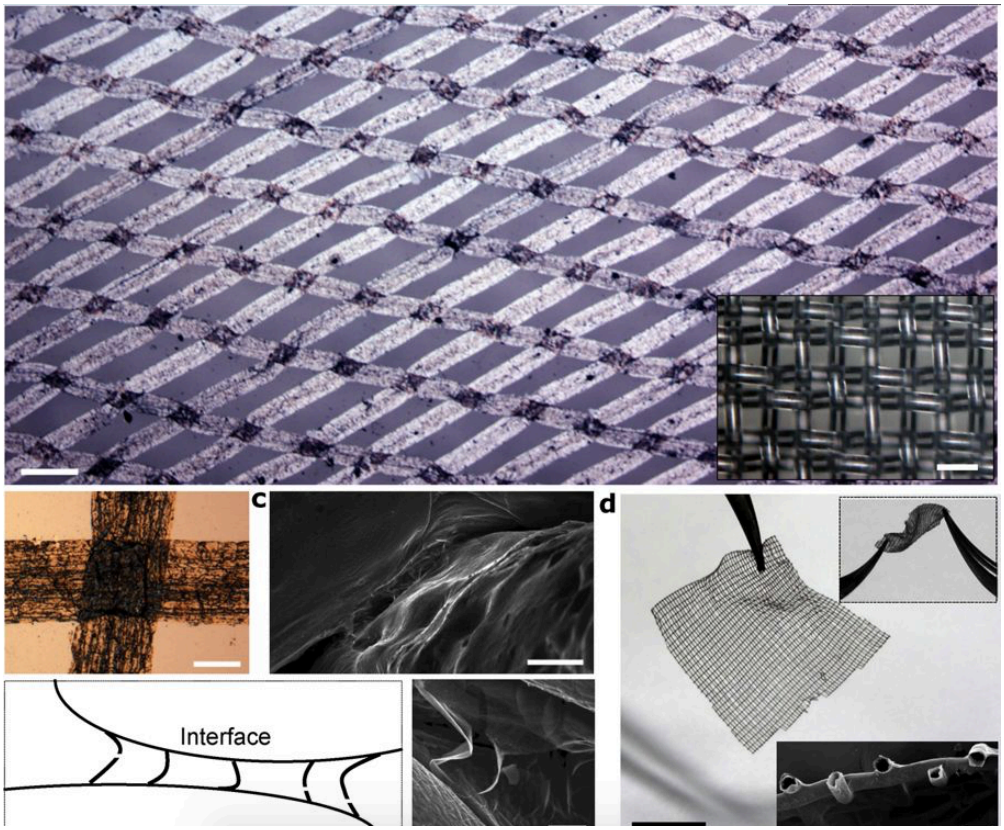

Fig 4.1: GWFs (Taken From - Li et. al 2012) [15]

A higher gauge factor implies that for identical values of mechanical stress, the resultant change in resistance is much higher. The gauge factor of graphene can be further increased through the creation of graphene meta-materials, where the electrical properties are not solely the result of the material's properties but also the result compositing the material into artificial structures. An example of such structural engineering was displayed in the works of Li et. al (2012) [15, 46], who created graphene woven fabrics (GWFs) by utilising a woven copper mesh as template for chemical vapour deposition (CVD) of graphene. The resultant sensor showed significant improvements over standard CVD films, notably in the 2-6% strain range, where the gauge factor equalled ~10^{3}. The other gains of this approach were realised in improved flexibility and strength of the sensor. Wang et al. (2010) [29] made use of the same approach to create their highly sensitive sensors.

The reason why GWFs perform better than standard sheets related to the density of deformations and their propagation through the structure under strain [15].

Even though GWFs are an excellent example of the use of graphene macrostructures, other approaches exist, such as Bai et al.'s (2010) [47] creation of a graphene nano-mesh to open a band gap in graphene through block copolymer lithography. In the absence of a CVD machine, the approach utilised by this project made use of a hybrid technique and tried to exploit the benefits presented by the methods presented above. The final process highlighted below was the result of several iterative steps which have been discussed in Appendix A.

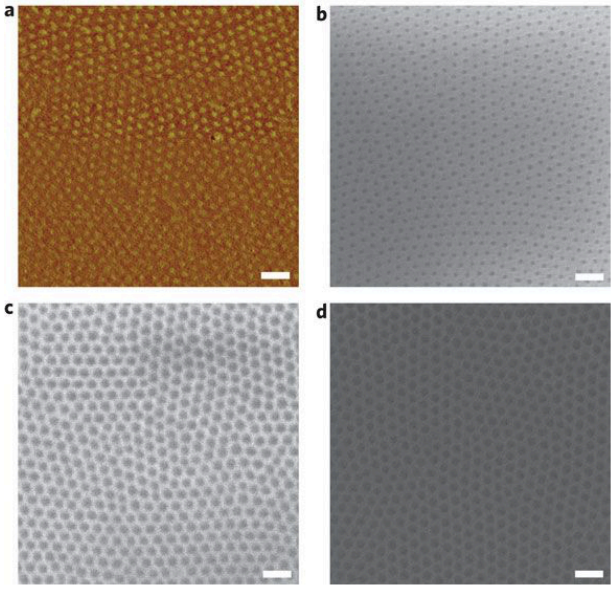

Fig 4.2: Graphene Nanomesh with 100nm scale bars (Taken from - Bai et al. 2010) [47]

CVD sheets of graphene on copper substrate, with dimensions of 1 inch x 1 inch were obtained from Graphenea [33].

These films came with a coating of Poly(methyl methacrylate) (PMMA). In order to create a mesh like structure, it was necessary to replace the PMMA coating with a photoresist, so that photolithography could be performed. S1813 photoresist was spun onto graphene after the removal of PMMA to carry out photolithography. A mesh with block width of $20\mu m$ was patterned using a laser writer. This was followed by a development step in MF319 and subsequently by oxygen

plasma etch to create holes in graphene. A second photolithography step followed to preserve small areas of copper on the back side from being etched away. This was done to ease the process of

Fig 4.3: Patterned graphene mesh on Cu

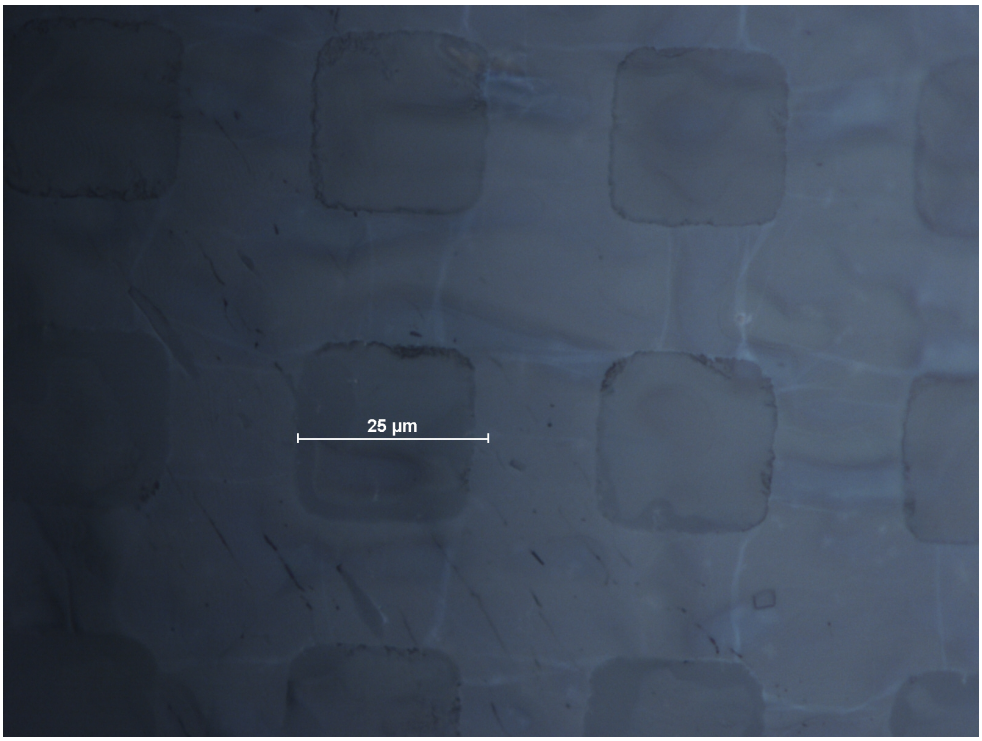

Fig 4.4: Graphene mesh after Cu etch (100X, dark field image)

contact application. Once the pattern was developed, the photoresist on top of graphene was removed and PMMA was spun on again to protect the sheet. The sheet was then placed PMMA-side-down on PDMS and the entire stack was deposited into a water based copper etch solution to remove the exposed copper.

After copper was etched, the stack was removed from the solution and washed in DI water before being treated by UV light inside a mask aligner to remove the resist from the contact edges. Finally, 2-point electrical contacts were applied using silver epoxy and the sensing area was covered with a piece of PDMS. The resultant stack is shown below, schematically and as a finished prototype.

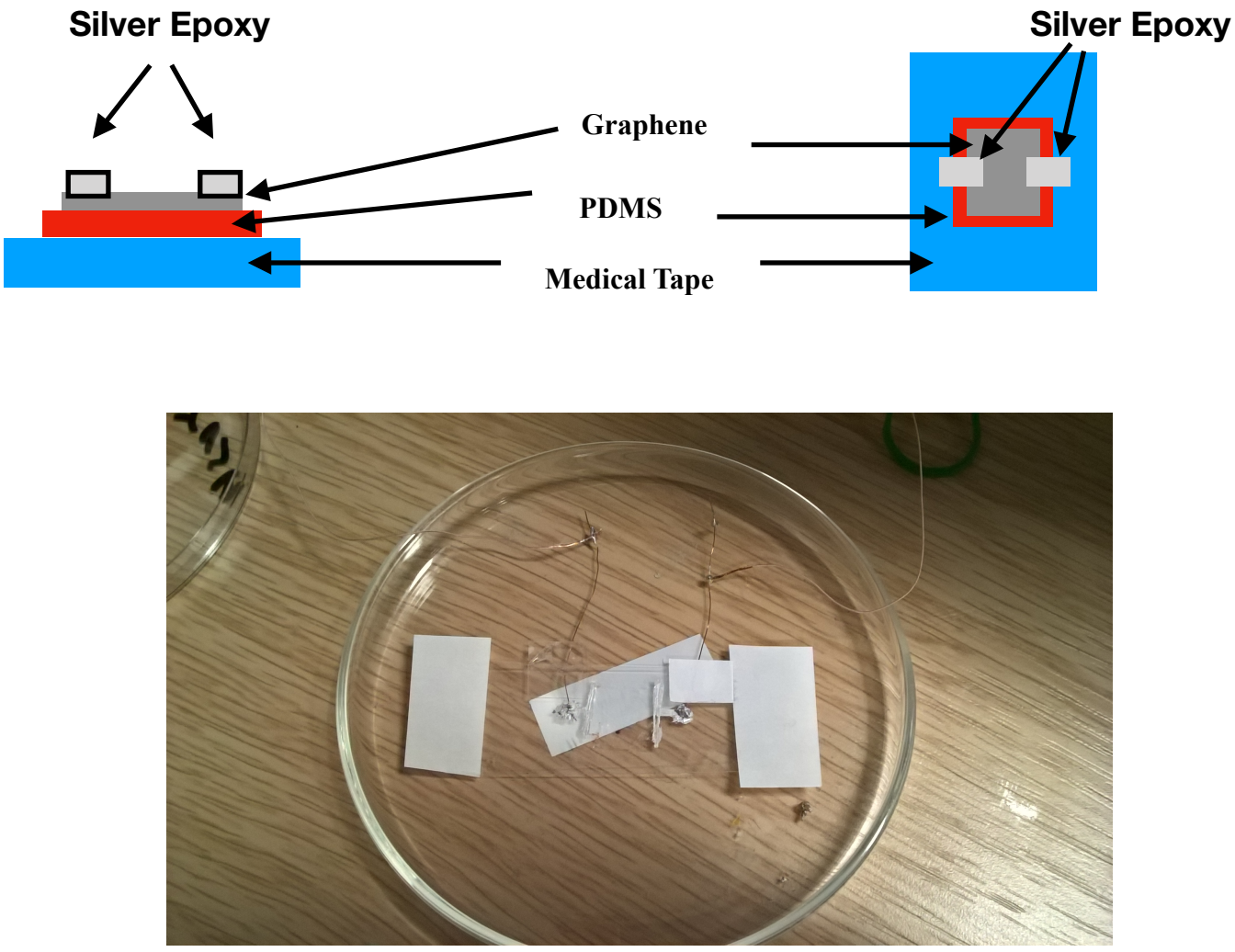

Fig 4.5: Sensor Stack Schematic (top) and prototype device (bottom)

4.2 Building the sensing and testing apparatus

4.2.1 Designing a test rig

Strain response of materials is often measured through a tension test. A tension test works by applying a uniaxial strain to the sample under test until it fails. The procedure is carried out using a universal testing machine, which either stretches the material under test or compresses it. However, such a machine wasn't available for this project and hence a custom solution had to be developed to suitably test the entire apparatus.

Three approaches were considered and two were built and tried out. The first one relied on using a pendulum that oscillated with a known frequency to graze the underside of the graphene sensor with a feather. In theory, it would have provided us with an increase in the resistance at fixed time intervals. Practically, three issues arose.

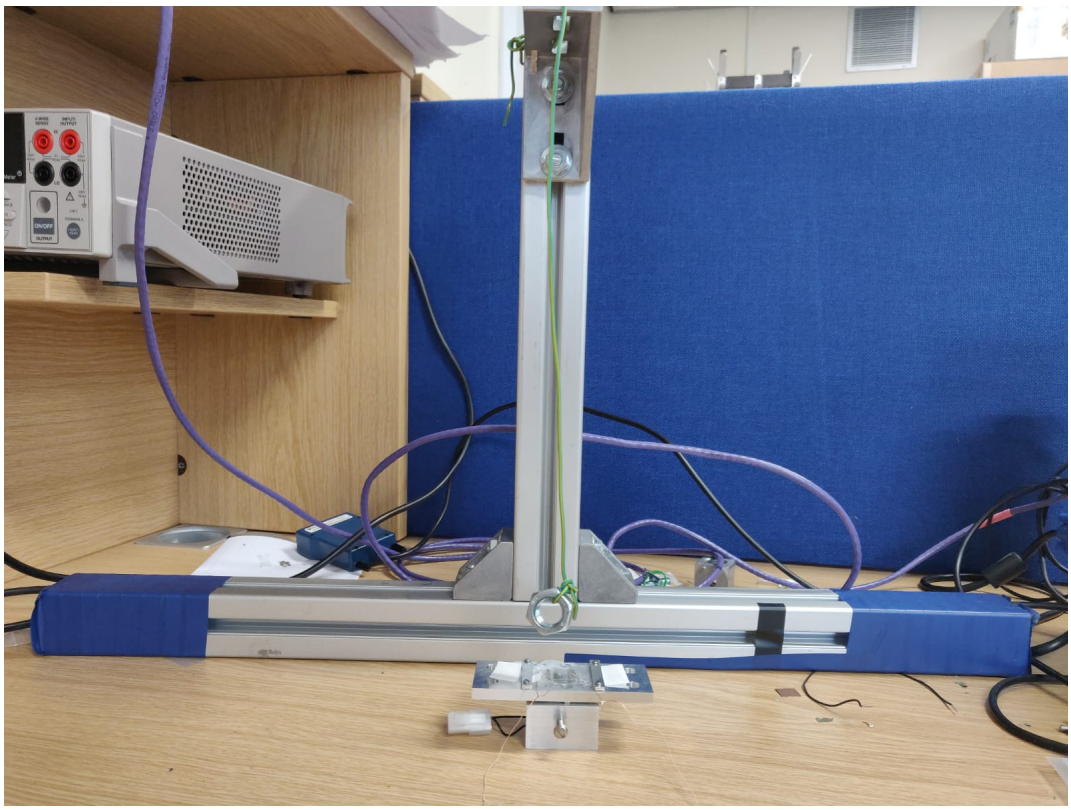

Fig 4.6: Pendulum Testing Rig

First, the application of the strain wasn't uniform, the trajectory of the pendulum was often altered by the scraping. Second, the strain applied wasn't enough to be detected on a nano-voltmeter like the Keithley 2400. Third, flipping the sensor over after attaching the contacts often ended up damaging the sensor or the contacts, thereby introducing extensive noise in the readings.

The second approach intended to polish the aforementioned approach. Instead of relying on a pendulum, we considered using a pulley driven by an Arduino to periodically raise and lower a known weight onto the sensor.

Again, theoretically, it relied on the same principle as the last one. Inspite of that, it didn't suffer from the non-uniformity of the strain application. While we didn't build and try this out, the design for this approach is given below.

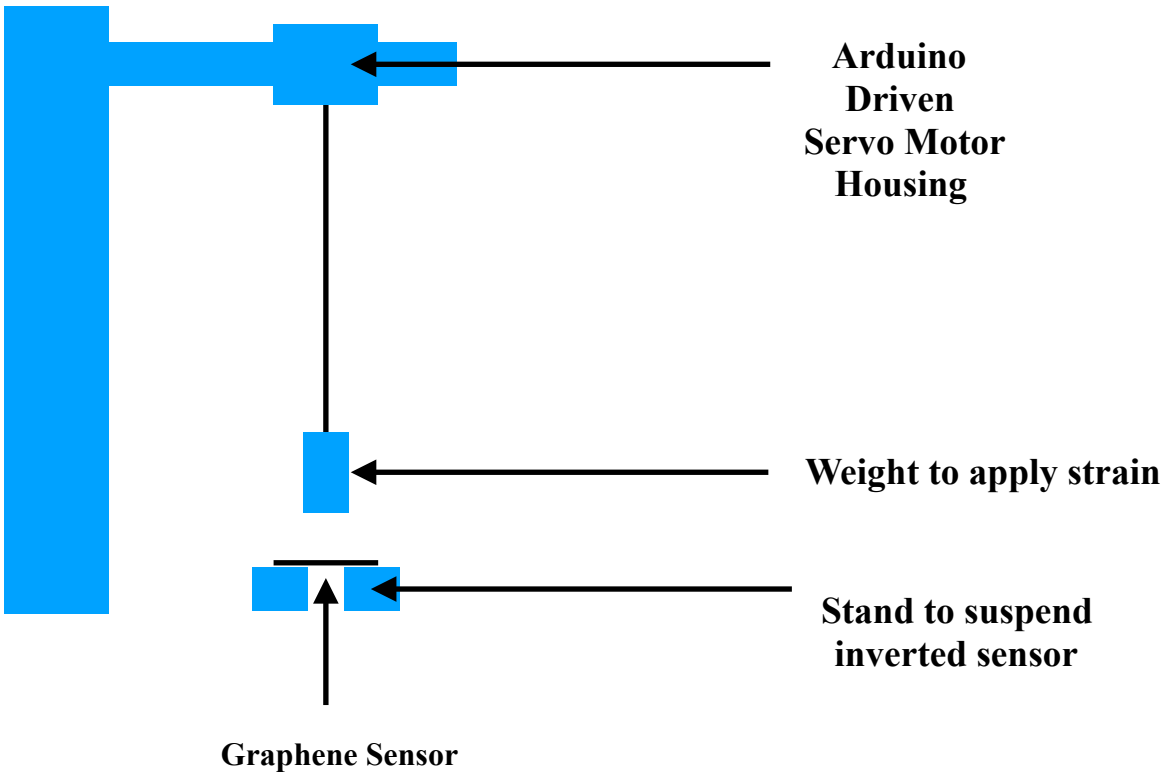

Fig 4.7: Pulley Driven System

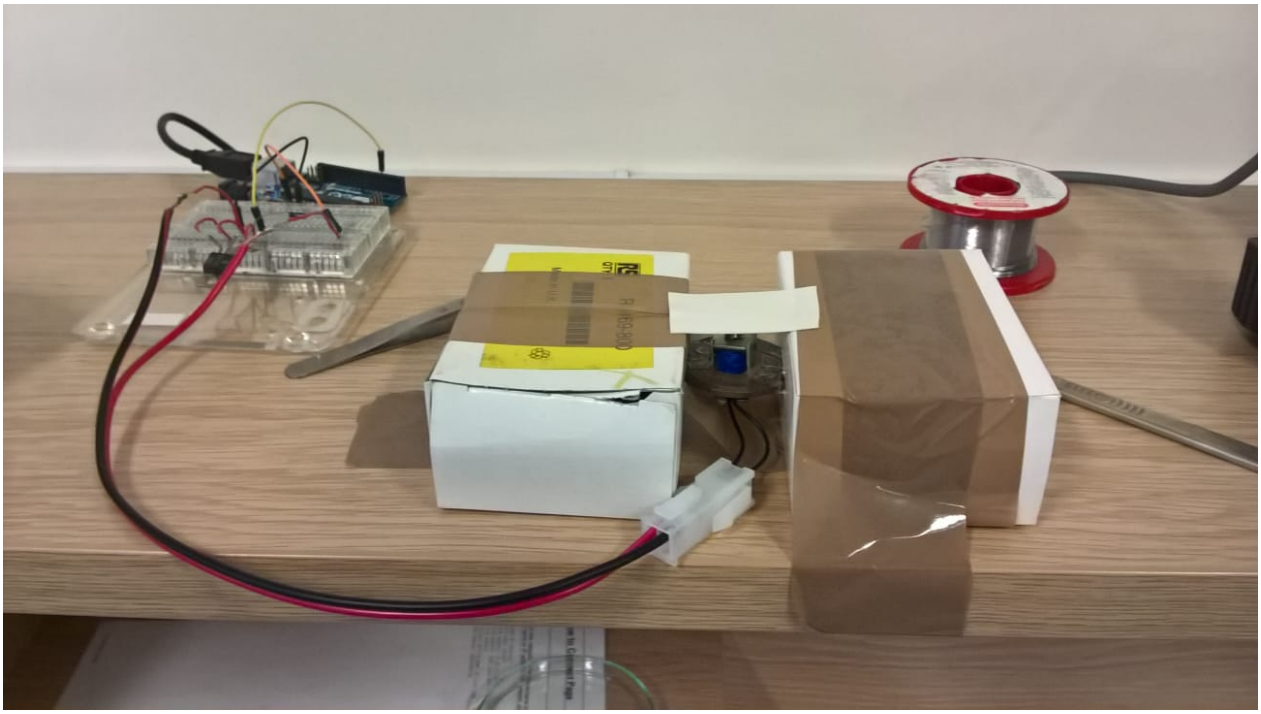

Fig 4.8: Arduino Driven Approach (v1.0)

The final design that was avoided all the problems mentioned above. It made use of an actuator driven by an Arduino Uno, driven at a constant frequency.

This actuator applied strain to the sensor that was suspended over an aperture and connected to the micro-controller/nano-voltmeter. One could also mimic the thickness of the human epidermis by

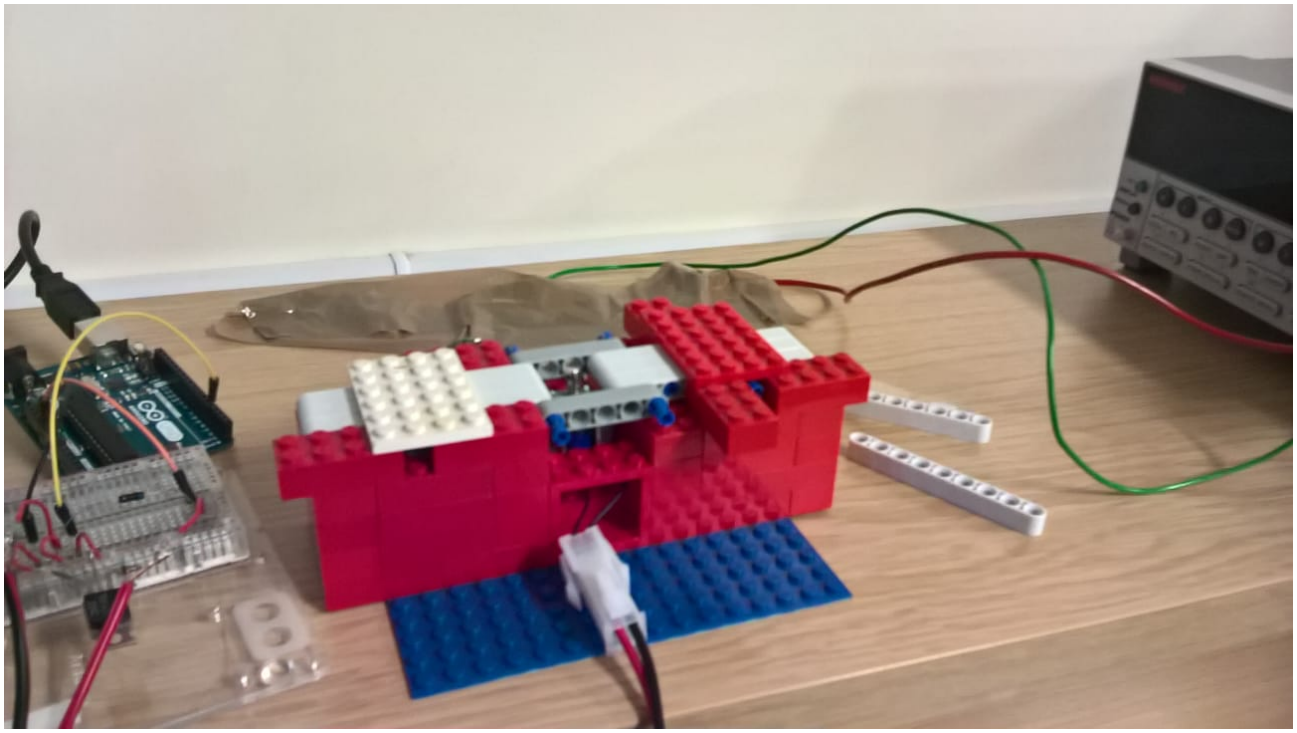

Fig 4.9: Arduino Driven Approach (v2.0)

suspending a polymer sheet over the aperture and attaching the sensor onto the polymer. This approach made testing repeatable. Since an Arduino Uno was used, it also became much easier to vary the frequency at which strain was induced.

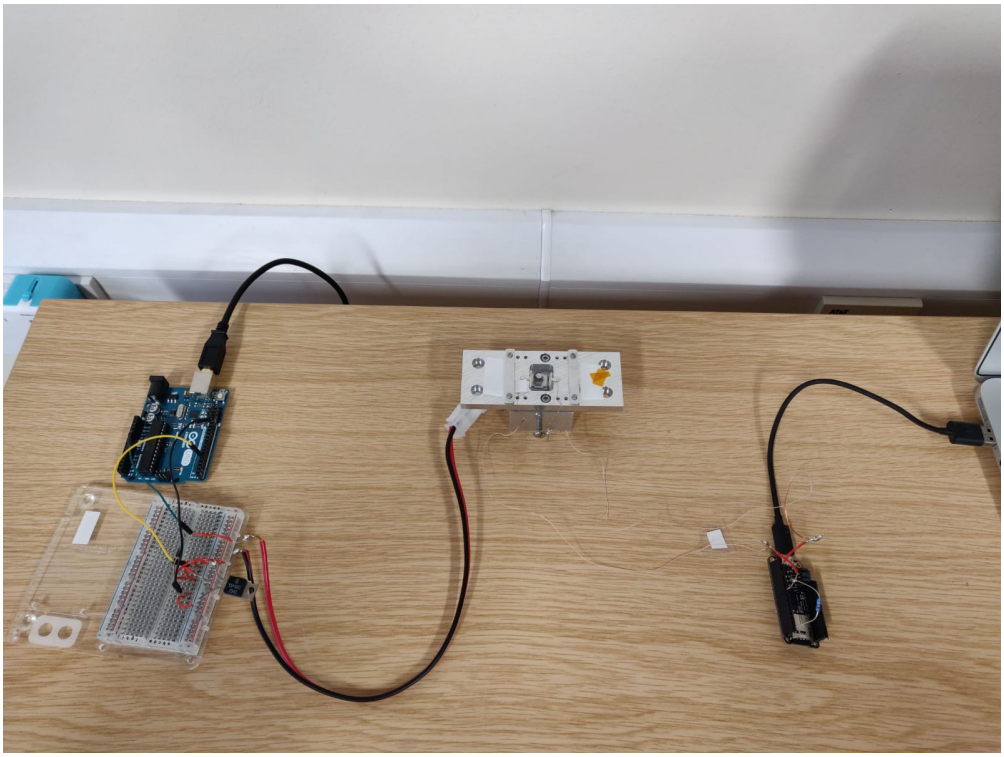

Fig 4.10: Arduino Driven Approach (v3.0)

4.2.2 Sensing Circuit

To measure the sheet resistance across graphene, a differential voltage measurement circuit had to be set up. This is motivated by the fact that a differential voltage measurement gives better readings than a single ended one when the signal source is noisy. The assumption of a noisy signal source is true in our case as the graphene sheet and to a certain extent, the contacts attached are a source of noise [48]. In addition to a differential measurement, we must also ensure that the voltage (across the graphene sensor) read in by the analog input is within the range of the ADC, else small changes in voltages won't be visible.

This can be achieved by using a voltage divider circuit that would make use of a reference resistor split the voltage between itself and the sensor, thereby keeping the voltage value in the expected range. An appropriate resistor can be identified by measuring the *at rest* resistance of the graphene sensor using a source meter. A resistor of approximately the same value as the sensor can then be chosen. These two observations gave rise to the following circuit. The diagram underneath shows the circuit design.

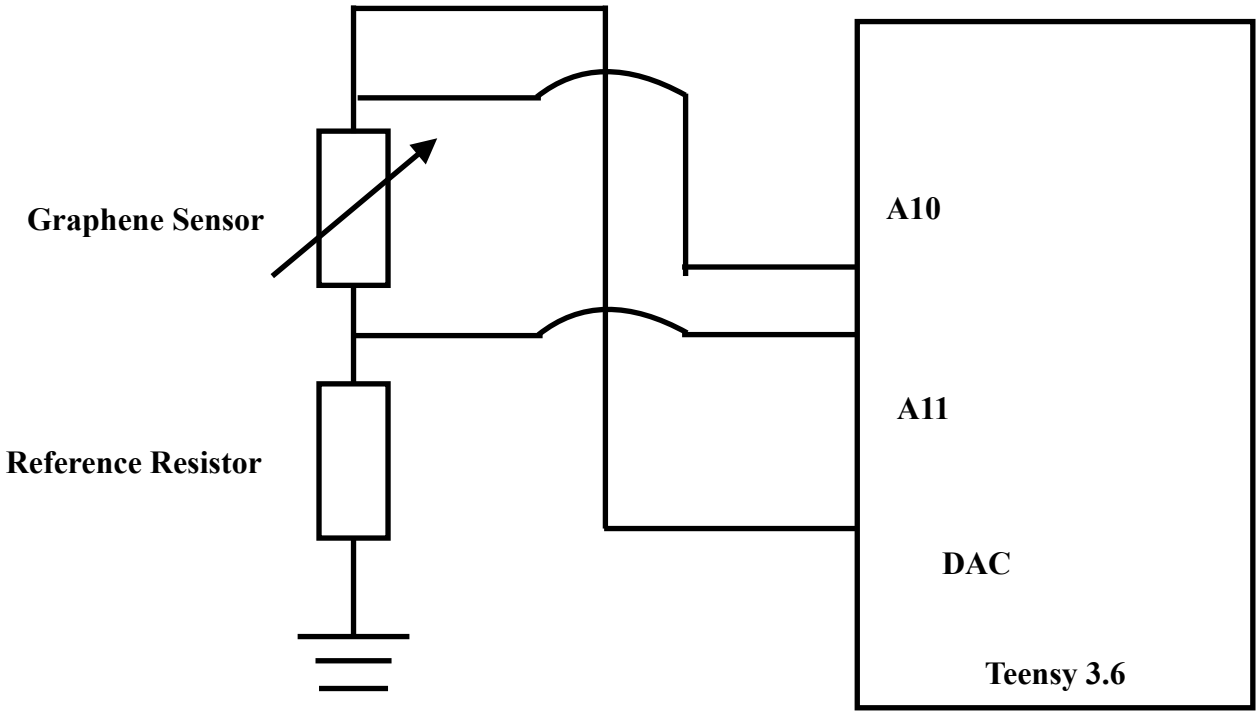

Fig 4.11: Circuit diagram for connecting the sensor to Teensy 3.6 to measure voltage changes

4.2.3 Testing Circuit

The main component in the testing circuit is the solenoid which has a voltage rating of 5V and a current rating (at same voltage) of 1.1A [49]. To drive this solenoid, the electromagnet must be switched on, which pulls the armature back. The large current necessitates the need of a power transistor to allow 1.1A of current to be delivered and to dissipate the resultant heat quickly.

As we would be switching the power on and off through the Arduino, we also need a diode that would protect the circuit's elements from damages during transient voltages. For the project's circuit, the transistor used was the TIP30C [50].

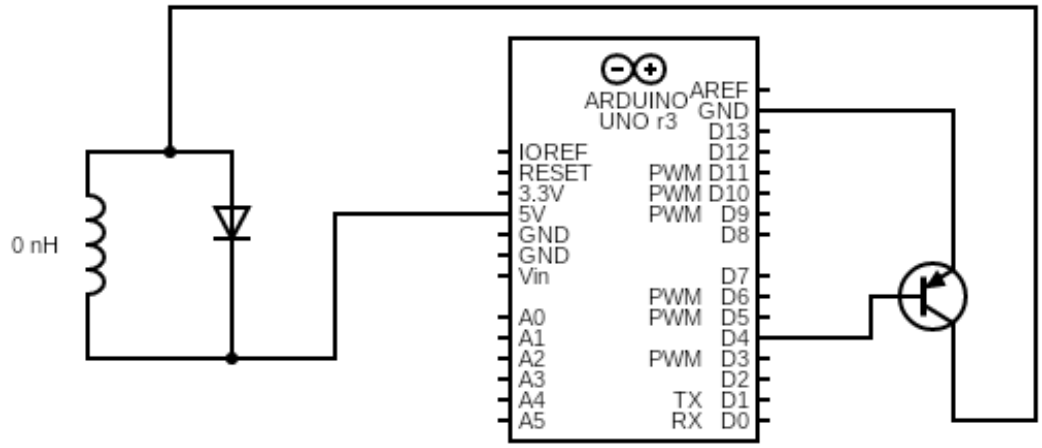

Fig 4.12: Circuit diagram for driving the actuator using an Arduino Uno to generate synthetic blinks

4.3 Implementing data collection and storage

4.3.2 Data Collection

To make full use of the ADC on the Teensy 3.6, Pedro Villanueva's ADC library [51] was used. This allowed for several customisable parameters such as changing the reference voltage, sampling speed and the type of measurement that must be taken. A lack of such functionality for the M0 data logger meant that the board couldn't be used. The configuration values for the ADC are provided in Appendix B. The result that was written to file was the average of 20 readings, which itself was the average of 100 samples that the ADC sampled.

4.3.3 Data Storage

The SD card library for the Arduino [52] makes use of the SdFat library [53] to handle IO. The SD library is programmed to flush the buffer after each write. Moreover, the `println()` function

performs a write for each digit in the number given to it. This causes the buffer to be flushed twice more in addition to the number of digits it has to write to file.

Since SD cards are read and written in 512 byte blocks by the virtue of their design [54], the SDFat library makes use of a single 512 byte buffer [55] to write data. When a flush occurs, the current block is written, the directory block on the card is read, updated and written, leading to 2048 bytes of IO.

In our application, we have to write the timestamp and the corresponding digital voltage value observed at that point. Now, assuming that the device is worn by a person during their waking hours, which can be approximately ~15 hours a day, this translates to $5.4E+07ms$, which can be represented using 26 bits, or 4 bytes. The digital voltage can be represented using an additional 2 bytes. 6 bytes of data and 2 new line statements imply we have 16,384 (8 * 2048) bytes of SD card IO for each line we write. Based on simple tests run by the SDFat library's creator, the write rate is about 77 bytes/sec [56]. In the same thread, the creator of SDFat writes that a higher write rate can be achieved by changing the SD card opening flag from `FILE_WRITE` to `O_CREAT | O_APPEND | O_WRITE`. This gives a write rate of 8571 bytes/sec and prevents the ADC's sampling rate from being affected.

4.3 Workflow

Once the data is written to the memory card, the only task that remains is to ensure that the physician can analyse it. This task is made simple by the Taverna workflow that expects the physician to add the raw data file as input, along with the patient ID.

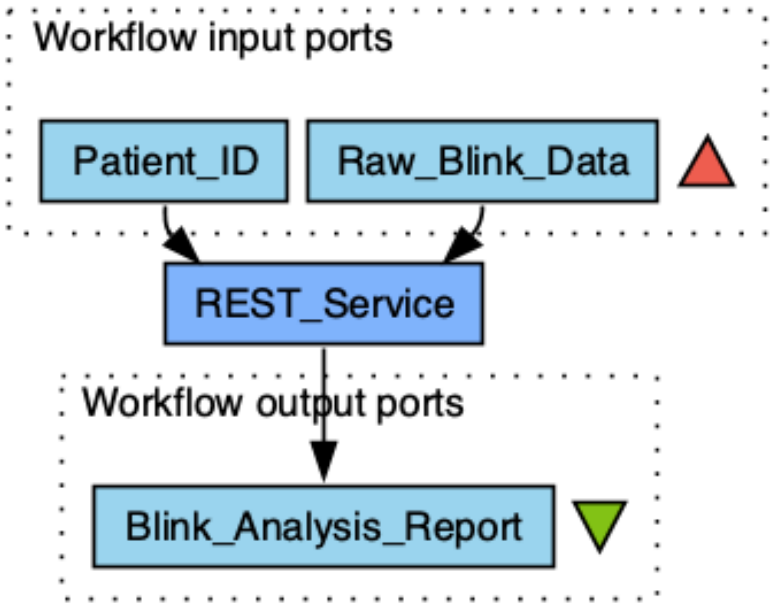

Fig 4.13: Taverna workflow to allow physicians to analyse blink data

This information is then sent to REST API endpoint which uses it to generate a PDF report emailed to the physician. The figure below shows the workflow in the Taverna environment. The most significant component is the REST_Service. This could have been easily written as a Python subprocess as well (which Taverna has provisions for).

This approach was avoided to ensure that the technical curve for the physicians isn't steep, since setting up the Python process to work correctly would require familiarity with virtual environments and pip installations. By using an API on the other hand, all of these details are abstracted away. More so, an API can easily be updated to allow for better analysis to take place and the updated analysis can much easily be propagated to several users.

4.4 API

The API was implemented in Python. It was made up of 3 sub-components. The first one carried out the raw data analysis. This component carried out a fast Fourier transform on the data to find the dominant frequency. One could use the dominant frequency to identify whether the blink trend is deviating from the normal and identify sources of noise in the sensor too. The FFT values also underpinned the rest of the analysis performed, such as identifying blink events in the data, computing the average blink rate for the duration of the data and the time between blinks.

The second component combined the results of the analysis into a PDF report. This PDF report was created using the *pylatex* library [57]. The report plotted the raw data and the corresponding frequency plot. It also had placeholders for values that would be clinically relevant, such as the Unified Parkinsons' Disease Rating Scale.

The final component sent out the report as an email using the smtplib library in Python.
The above components were access through an API endpoint set up using Flask, which allows for custom routes to be created. The flask endpoint accepted post requests with a patient ID and on successful generation of the report, sent back a 200 OK status to Taverna.

For the purpose of this project, the API was hosted locally. However, it was designed with online hosting, on a service like Heroku or AWS, in mind. As a result, the package dependencies were managed through a virtual environment that could easily be replicated in a cloud based hosting provider.

Report for Patient 1

March 1, 2019

Average Blink Rate (Blinks per minute)	Average Time Between Blinks
40	332

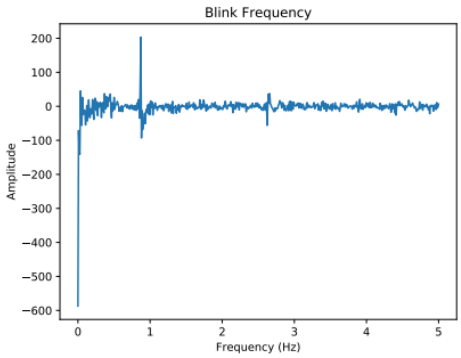

Figure 1: Blink Frequency

Voluntary Blinks / minute	Involuntary Blinks / minute	Spontaneous Blinks / minute
800	200	100

1

Fig 4.14: Sample report snippet generated by the API on analysis of synthetic blink data

5. Testing and Results

5.1 Sensor Iterations and Results

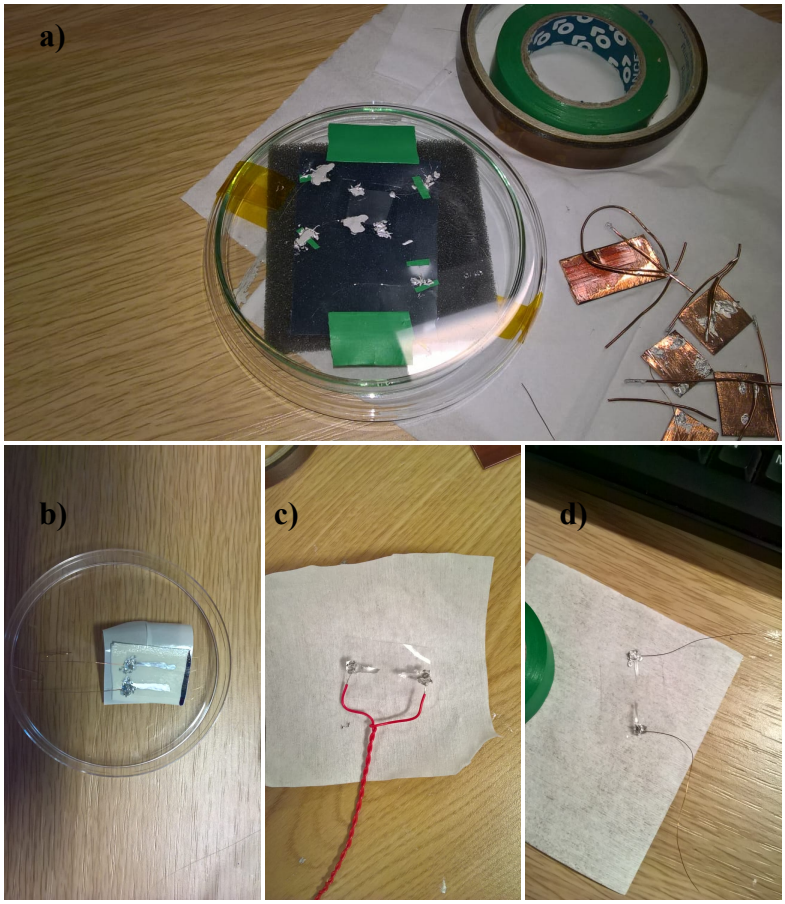

Fig 5.1 **a)** Graphene sensor using gold wires and 4-point contacts **b)** Graphene sensor with silver paint channels and 2-point copper wire contacts on surgical tape **c)** Graphene sensor on PDMS with aluminium wires **d)** Graphene sensor on PDMS with conductive thread

The sensor whose results are displayed below was the product of several design iterations. Each of the sensors preceding the final one were tested using the Keithley 2400 before they were tested, if at all, using the micro controller. While the fabrication process for each of these sensors remained

mostly unchanged, they each utilised an improved contact process and/or uses of wires of different flexibility. It was found out here that aluminium wires, which prevented the sensor from folding it on itself, were quite inflexible when it came it attaching it to a polymer surface. Most of these iterations suffered from contact fragility, which caused them to come apart due to mechanical strain, sometimes even before the tests. For the earlier iterations, where the contacts were directly attached onto graphene, this also represented damage to the structure of the sheet.

Later, it meant higher resistance as the channels made out of silver paint started cracking.

5.2 Bench Tests and Results

Bench tests to evaluate sensor prototypes were carried out using the Keithley 2400 nano-voltmeter. The source voltage was set to 0.1V and the current across the graphene sheet was measured. Data was recorded using LabView. This procedure was repeated whilst the sensors were unstrained and under strains imposed by the actuator. Unstrained resistance values helped establish the baseline value, R_0 for each sensor, which was later used to calculate change over baseline using the formula $\Delta R = \frac{R_t - R_0}{R_0}$, where R_t is the resistance across the sheet at time t. A plot of the resultant resistance values and its corresponding power spectral density plot, with a peak frequency of 1Hz (actuator's stimulus frequency) is shown underneath.

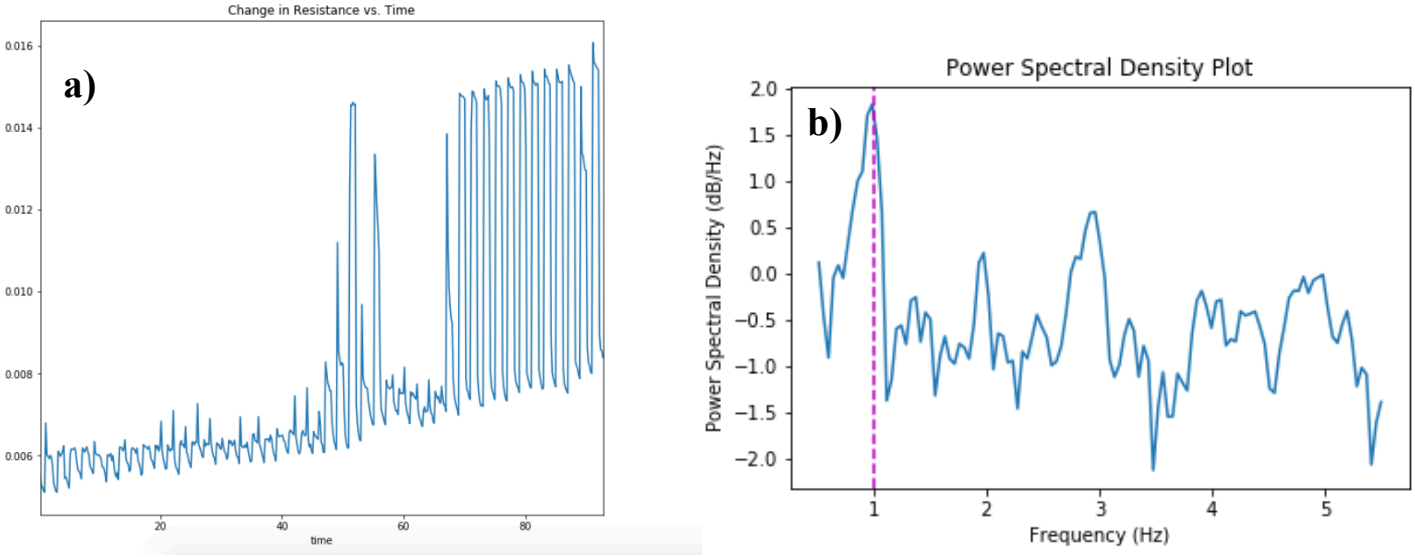

Fig 5.1: **a)** Change in resistance measured on the Keithley 2400 with a 1Hz stimulus **b)** Corresponding Power Spectral Density plot

5.3 End to End Tests and Results

End to end tests made use of the Teensy 3.6 for measuring differential voltage instead of the current. This choice was made since the board was able to provide a voltage source through its DAC pin. Two sorts of tests were performed, in the first, the data was collected while stimulus was applied at a constant frequency of 1Hz. This was then changed to a variable frequency relying on a 3 phase model. The first phase, which starts with the solenoid fully extended, was the eyes closed phase. The second phase was the start of the opening movement and the closed eye phase and the last phase was a transition into a completely open position. The idea behind designing this text fixture was to simulate the asymmetric nature of eye blinking in the absence of human test subjects.

The delay values for each of these phases were calculated by using a normal distribution of time periods obtained from Agostino et al.'s (2008) [3] work. All the data was stored on the memory card and then put through the pipeline to get the resulting reports for each of the tests. The collected data is visualised below.

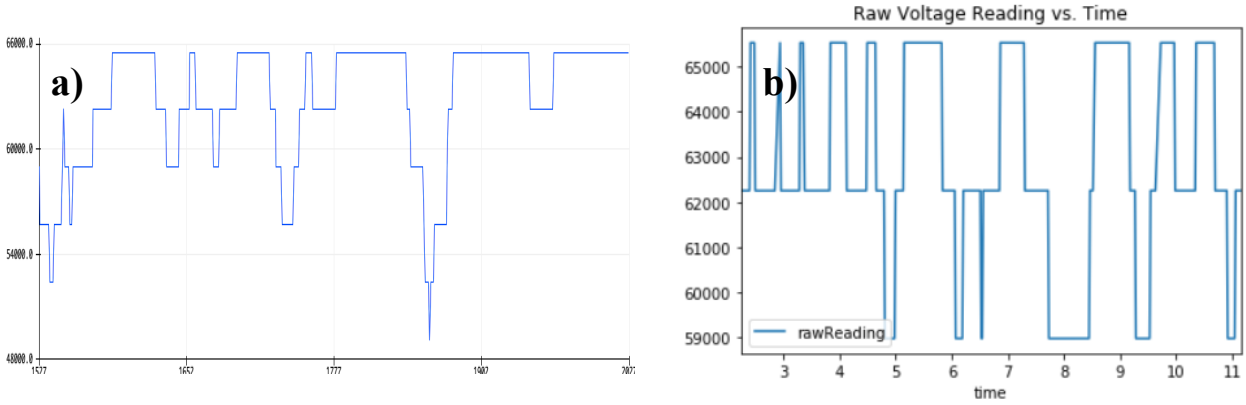

Fig 5.2: Electrical measurements obtained on the Teensy 3.6 by applying **a)** 1Hz stimulus **b)** asymmetric stimulus using an Arduino Uno driven actuator.

6. Conclusion and Reflection

6.1 Conclusion

This project was able to successfully build a proof of concept that showed that graphene can indeed be used in the detection of synthetic eye blinks. It also goes on to show that these eye blinks can be picked up on a low cost micro-controller which can easily be integrated into a wearable system that allows for unobtrusive monitoring. Finally, it demonstrates that the entire process of data analysis can be automated to aid the physician's assessment of the disease.

Although the sensor couldn't be tested on actual human subjects, it overcame several technical challenges that otherwise restricted sensors of such type from prolonged usage. For instance, much more robust electrical contacts were developed that prevented the sensors from coming apart after a few strain cycles. Altogether, it paved a strong foundation for exciting future work that can be undertaken in this domain. Some examples of this have been discussed in Section 6.3.

6.2 Planning and Management

At the very start, I was aware of the fact that this project represented a very steep learning curve, since I planned on delving into a domain that was far removed from Computer Science.

For this reason, before the start of Semester 1, I decided to get acquainted with the various techniques necessary for device fabrication at the Centre for Mesoscience and Nanotechnology. Initially, the project was hinged on following the methods of Wang et al. (2014) [29] and I expected that we'd be able to reproduce their results. This initial stage was expected to be done by October, and the plan from that point onwards was to try and make the sensors mechanically robust, in time for human trials in the second semester.

This plan had to be revised since we were unable to access a CVD machine and tried to achieve the intended results using graphene films, which didn't seem to work at first until we changed our fabrication method. Under the revised plan, it became necessary to first develop a good testing strategy for carrying out bench tests and and then overcome the issue with mechanically flimsy contacts that were often a huge source of noise. While these represented setbacks in the overarching plan, they did help me solve fundamental issues that would be useful in any future work I undertake in this field.

In case I had to do things differently, I would have run an experiment to compare the various gauge factors as the sensor design varied instead of relying on subjective evaluations presented in the literature. In addition to that, I would have liked to test out the effect of removing the PMMA layer in our stack and investigate whether that improves the strain response. Likewise, testing different wires and interconnects (2-point or 4-point measurements) would have provided us with more

flexibility and/or sensitivity. It would have also been possible to improve the circuit design so that even smaller voltage changes could be picked up, by using an operational amplifier, for instance. Based on these results, it might have been possible to make even more sensitive sensors.

6.3 Future Work

There is a vast array of future work that can be undertaken along the same lines of inquiry as this project. The most direct line of inquiry is utilising the improved, robust contact techniques and the use of a low cost micro controller to conduct longitudinal studies with GWFs to establish the utility of these devices in real world settings. Once that is established and the sensors are indeed found to be useful, then a comparison of various materials could be undertaken to determine what makes for the most cheapest, unobtrusive and easy to use sensor in such contexts. Further work could be undertaken to make these sensors more unobtrusive by building them as RFID tags, similar to the work done by Leng et al. (2016) [58] with graphene on paper substrates. Another approach could possibly look into detecting blinks as a function of light intensity, by relying on transition metal dichalcogenides, such as MoS_2 which is known to have ultrafast response to changes in light intensity [59].

The result of these investigations can then be applied to other neurodegenerative diseases that display similar eye blink kinematics, improving diagnostic and monitoring abilities.

Appendix A

Sensor Fabrication Process

1. Use O2 Plasma etch to carry out a 45s etch on the Copper side of the CVD sheet to remove graphene flakes.
2. Remove PMMA from the top of the CVD sheet by a 10 minute submersion in Acetone followed by a 10 minute submersion in IPA. Initially, this step was unnecessary since we planned on working with un-patterned films and decided to use the PMMA layer as an adhesive for firmer contact with the PDMS layer.
3. Spin on S1813 photoresist using a spin-coater at 3000RPM for 60s.
4. Bake the sample for 2 minutes at 110°C.
5. Using a laser writer, patter a mesh like structure with squares at a distance of 20-50μm. 30% filter, d-step of 8 and all the gain worked in our case.
6. Develop the pattern using MF319 immersion for 30s followed by water immersion for another 30s.
7. Using O2 Plasma for 1 minute on the photoresist side, to remove exposed graphene.
8. Remove S1813 using Acetone and spin on PMMA at same spin settings at earlier.
9. Bake sample for 5 minutes at 170°C.
10. On the copper side, spin on S1813 for patterning contact edges.
11. Pattern a box using a laser writer (same settings as before to expose and active area for blink sensing. Develop pattern as usual.
12. Attach CVD sheet to PDMS with PMMA side facing down and hold it in place using 3M's 2477P to prevent CVD sheet detachment during copper etch.
13. Prepare copper etch using 2.5g ammonium persulfate and 100ml DI water.

14. Leave CVD sheet for at least 12 hours in Cu etch, with the copper side facing the edge.
15. Remove S813 using UV exposure in the mask aligner and MF319.
16. Attach wires to copper contact edge using silver epoxy and bake in oven for 15 minutes at 65°C.

Initially, the process was much simpler since no patterning was involved. However, contacts were initially attached to the exposed graphene surface using silver paint. While silver paint worked well for short trials, it often came off during prolonged usage and damaged the graphene sheet. The first step to change this was to build sensors where a conducting channel using silver paint was painted on PDMS and contacts were attach off the graphene sheet on PDMS using epoxy, as shown in the figure below. This still wasn't as sturdy since silver epoxy's adhesion to polymers is weaker than its adhesion to metals. By leaving some un-etched copper edges, we were able to exploit silver epoxy's adhesion to metals to make stronger contacts. An obvious way of removing the contact noise would have been through 4-point measurements, yet, in order to keep the circuit simple and to allow easy application of sensor, that was avoided.

Appendix B

The ADC settings used on the Teensy 3.6 were:

- **Reference Voltage:** 1.2V
- **Averaging:** 100
- **Resolution:** 16 bits
- **Conversion Speed:** Medium
- **Sampling Speed**: High

References

1. “2015 Vision.” *Blinking*, www.d.umn.edu/~jfitzake/Lectures/DMED/Vision/Optics/Blinking.html.
2. Tong, John. “Anatomy, Head and Neck, Eye Orbicularis Oculi Muscle.” StatPearls [Internet]., U.S. National Library of Medicine, 19 Sept. 2018, www.ncbi.nlm.nih.gov/books/NBK441907
3. Agostino, Rocco, et al. “Voluntary, Spontaneous, and Reflex Blinking in Parkinson's Disease.” *Movement Disorders*, vol. 23, no. 5, 2008, pp. 669-675. *Wiley*, doi:10.1002/mds.21887
4. Surmeier, D. James, et al. “What Causes the Death of Dopaminergic Neurons in Parkinson’s Disease?” *Progress in Brain Research Recent Advances in Parkinson’s Disease: Basic Research*, vol. 183, 2010, pp. 59–77. *Elsevier,* doi:10.1016/s0079-6123(10)83004-3.
5. Galvan, Adriana, and Thomas Wichmann. “Pathophysiology of Parkinsonism.” Clinical Neurophysiology, vol. 119, no. 7, July 2008, pp. 1459–1474. *Elsevier BV,* doi:10.1016/j.clinph.2008.03.017.
6. Graybiel, AM. “The Basal Ganglia.” *Cell*, 2000, www.cell.com/current-biology/pdf/S0960-9822(00)00593-5.pdf.
7. Calabresi, Paolo, et al. “Direct and Indirect Pathways of Basal Ganglia: a Critical Reappraisal.” *Nature Neuroscience*, vol. 17, no. 8, 2014, pp. 1022–1030. *Springer Nature,* doi:10.1038/nn.3743.
8. Novoselov, K. S., et al. “Two-Dimensional Atomic Crystals.” *Proceedings of the National Academy of Sciences*, vol. 102, no. 30, 2005, pp. 10451–10453. doi:10.1073/pnas.0502848102.
9. Novoselov, K. S. “Electric Field Effect in Atomically Thin Carbon Films.” *Science*, vol. 306, no. 5696, 2004, pp. 666–669. *Proceedings Of The National Academy of Sciences,* doi:10.1126/science.1102896.

10. Geim, A. K., and K. S. Novoselov. “The Rise of Graphene.” *Nature Materials*, vol. 6, no. 3, 2007, pp. 183–191. *Springer Nature,* doi:10.1038/nmat1849.

11. “Silicon.” *Electrical Properties of Silicon (Si)*, www.ioffe.ru/SVA/NSM/Semicond/Si/electric.html.

12. Schwierz, Frank. “Graphene Transistors.” *Nature Nanotechnology*, vol. 5, no. 7, 2010, pp. 487–496. doi:10.1038/nnano.2010.89.

13. Nair, R. R., et al. “Fine Structure Constant Defines Visual Transparency of Graphene.” *Science*, vol. 320, no. 5881, 2008, pp. 1308–1308. *American Association for the Advancement of Science (AAAS)*, doi:10.1126/science.1156965.

14. Lee, C., et al. “Measurement of the Elastic Properties and Intrinsic Strength of Monolayer Graphene.” *Science*, vol. 321, no. 5887, 2008, pp. 385–388. *American Association for the Advancement of Science,* doi:10.1126/science.1157996.

15. Li, Xiao, et al. “Stretchable and Highly Sensitive Graphene-on-Polymer Strain Sensors.” *Scientific Reports*, vol. 2, no. 870, 2012. *Springer Nature,* doi:10.1038/srep00870.

16. Frigerio, Alice, et al. "Infrared-based blink-detecting glasses for facial pacing: toward a bionic blink." *JAMA facial plastic surgery,* vol. 16, no. 3, 2014, pp. 211-218. *American Medical Association (AMA)*, doi:10.1001/jamafacial.2014.1

17. Smith, P., et al. “Monitoring Head/Eye Motion for Driver Alertness with One Camera.” *Proceedings 15th International Conference on Pattern Recognition. ICPR-2000*, 3 Sept. 2000, doi:10.1109/ICPR.2000.902999.

18. Fan, Xiao, et al. “Yawning Detection for Monitoring Driver Fatigue.” *2007 International Conference on Machine Learning and Cybernetics*, vol.2, 2007, pp. 664 - 668. doi:10.1109/icmlc.2007.4370228.

19. Fan, Xiao, et al. “Yawning detection based on gabor wavelets and LDA”, *Journal of Beijing University of Technology*, 2009, pp. 409–413.

20. Bhardwaj, Abhishek, et al. “Image filtering techniques used for monitor driver fatigue: a survey.” *International Journal of Scientific and Research Publications*, 2013, pp. 1–4.

21. Dementyev, Artem, and Christian Holz. “DualBlink.” *Proceedings of the ACM on Interactive, Mobile, Wearable and Ubiquitous Technologies*, vol. 1, no. 1, 2017, pp. 1–19. *Association for Computing Machinery (ACM),* doi:10.1145/3053330.

22. Rushworth, G. “Observations On Blink Reflexes.” *Journal of Neurology, Neurosurgery & Psychiatry*, vol. 25, no. 2, 1962, pp. 93–108. *BMJ,* doi:10.1136/jnnp.25.2.93.

23. Kimura, Jun. “Disorder Of Interneurons In Parkinsonism.” *Brain*, vol. 96, no. 1, 1973, pp. 87–96. doi:10.1093/brain/96.1.87.

24. Basso, Michele A., et al. “An Explanation for Reflex Blink Hyperexcitability in Parkinson’s Disease. I. Superior Colliculus.” *The Journal of Neuroscience*, vol. 16, no. 22, 1996, pp. 7308–7317. doi:10.1523/jneurosci.16-22-07308.1996.

25. Karson, Craig N. “Spontaneous Eye-Blink Rates And Dopaminergic Systems.” *Brain*, vol. 106, no. 3, 1983, pp. 643–653. doi:10.1093/brain/106.3.643.

26. Jongkees, Bryant J., and Lorenza S. Colzato. “Spontaneous Eye Blink Rate as Predictor of Dopamine-Related Cognitive Function—A Review.” *Neuroscience & Biobehavioral Reviews*, vol. 71, 2016, pp. 58–82. *Elsevier BV*, doi:10.1016/j.neubiorev.2016.08.020.

27. Dagdeviren, Canan, et al. “Recent Progress in Flexible and Stretchable Piezoelectric Devices for Mechanical Energy Harvesting, Sensing and Actuation.” *Extreme Mechanics Letters*, vol. 9, 2016, pp. 269–281. *Elsevier BV*, doi:10.1016/j.eml.2016.05.015.

28. Lee, Sangmin, et al. “Super-Flexible Nanogenerator for Energy Harvesting from Gentle Wind and as an Active Deformation Sensor.” *Advanced Functional Materials*, vol. 23, no. 19, 2012, pp. 2445–2449. *Wiley*, doi:10.1002/adfm.201202867.

29. Wang, Yan, et al. “Wearable and Highly Sensitive Graphene Strain Sensors for Human Motion Monitoring.” *Advanced Functional Materials*, vol. 24, no. 29, 2014, pp. 4666–4670. *Wiley,* doi: 10.1002/adfm.201400379.

30. Yamada, Takeo, et al. “A Stretchable Carbon Nanotube Strain Sensor for Human-Motion Detection.” *Nature Nanotechnology*, vol. 6, no. 5, 2011, pp. 296–301. *Springer Nature*, doi: 10.1038/nnano.2011.36.

31. Yin, Gang, et al. “A Carbon Nanotube/Polymer Strain Sensor with Linear and Anti-Symmetric Piezoresistivity.” *Journal of Composite Materials*, vol. 45, no. 12, 2011, pp. 1315–1323. *SAGE Publications*, doi:10.1177/0021998310393296.

32. Yang, Wenrong et al. "Carbon Nanomaterials In Biosensors: Should You Use Nanotubes Or Graphene?". *Angewandte Chemie International Edition*, vol 49, no. 12, 2010, pp. 2114-2138. *Wiley,* doi:10.1002/anie.200903463.

33. “Monolayer Graphene on Cu with PMMA Coating.” *Graphenea*, www.graphenea.com/collections/graphene-products/products/monolayer-graphene-on-cu-with-pmma-coating-4-inches?variant=51789741779.

34. “PDMS.” *PDMS*, www.mit.edu/~6.777/matprops/pdms.htm.

35. *3M™ 2476P Polyester Spunlace Nonwoven Fabric Medical Tape*. *3M™ 2476P Polyester Spunlace Nonwoven Fabric Medical Tape*, 3M, www.3m.com/3M/en_US/company-us/all-3m-products/~/3M-2476P-Spunlaced-Polyester-Nonwoven-Fabric-Medical-Tape/?N=5002385+8729803+3294739650&rt=rud&utm_campaign=lead_find_my_adhesive&utm_medium=one&utm_source=oe&utm_content=pdp&utm_term=hcbg-c3sd-meddevice-en_us-lead-find_my_adhesive-one-oe-na-pdp-na-apr18.

36. 3M™ 1522 Transparent Polyethylene Double Sided Medical Tape, 80 # Liner. 3M™ 1522 Transparent Polyethylene Double Sided Medical Tape, 80 # Liner, 3M.

37. 3M™ 2477P Double-Coated TPE Silicone Acrylate Medical Tape with Premium Liner. 3M™ 2477P Double-Coated TPE Silicone Acrylate Medical Tape with Premium Liner, 3M.
38. Adafruit, "Adafruit Feather M0 Adalogger", Atmel SAM D21E / SAM D21G / SAM D21J Datasheet, 2015
39. Freescale Semiconductor, Inc., “Teensy 3.6”, Kinetis K66 Sub-Family Datasheet, 2016
40. “AnalogReference().” *Arduino Reference*, www.arduino.cc/reference/en/language/functions/analog-io/analogreference/.
41. Beauchemin, Maxime, et al. “Apache Airflow.” *Apache Airflow*, 1.10.3, 2014, airflow.apache.org/project.html.
42. Wolstencroft, Katherine, et al. “The Taverna Workflow Suite: Designing and Executing Workflows of Web Services on the Desktop, Web or in the Cloud.” *Nucleic Acids Research*, vol. 41, no. W1, 2013, pp. W557–W561. *Oxford University Press (OUP)*, doi:10.1093/nar/gkt328.
43. Goble, Carole A., et al. “MyExperiment: a Repository and Social Network for the Sharing of Bioinformatics Workflows.” *Nucleic Acids Research*, vol. 38, no. suppl_2, 2010, pp. W677–W682. *Oxford University Press (OUP)*, doi:10.1093/nar/gkq429.
44. Lee, Youngbin, et al. “Wafer-Scale Synthesis and Transfer of Graphene Films.” *Nano Letters*, vol. 10, no. 2, 2010, pp. 490–493. *American Chemical Society (ACS)*, doi:10.1021/nl903272n.
45. Chiriac, Horia, et al. “Ni–Ag Thin Films as Strain-Sensitive Materials for Piezoresistive Sensors.” *Sensors and Actuators A: Physical*, vol. 76, no. 1-3, 1999, pp. 376–380. *Elsevier BV*, doi:10.1016/s0924-4247(99)00027-8.
46. Li, Xiao, et al. “Multifunctional Graphene Woven Fabrics.” *Scientific Reports*, vol. 2, no. 1, 2012. *Springer Nature*, doi:10.1038/srep00395.
47. Bai, Jingwei, et al. “Graphene Nanomesh.” *Nature Nanotechnology*, vol. 5, no. 3, 2010, pp. 190–194. *Springer Nature,* doi:10.1038/nnano.2010.8.

48. Rumyantsev, S, et al. “Electrical and Noise Characteristics of Graphene Field-Effect Transistors: Ambient Effects, Noise Sources and Physical Mechanisms.” *Journal of Physics: Condensed Matter*, vol. 22, no. 39, 2010, p. 395302. *IOP Publishing*, doi: 10.1088/0953-8984/22/39/395302.
49. Adafruit Industries. “Mini Push-Pull Solenoid - 5V.” *Adafruit Industries Blog RSS*, www.adafruit.com/product/2776.
50. ON Semiconductor, “TIP30C PNP Epitaxial Silicon Transistor”, TIP30C Datasheet, 2014
51. Villanueva, Pedro. “ADC.” *Github*, Oct. 2013, github.com/pedvide/ADC.
52. Greiman, William, and Sparkfun Electronics. “SD Library for Arduino.” *Github*, 2009, github.com/arduino-libraries/SD.
53. Greiman, William. “Arduino FAT16/FAT32 Library.” *Github*, 2014, github.com/greiman/SdFat.
54. Greiman, William. “SdSpiCard.h.” Github, 2019, 54. https://github.com/greiman/SdFat/blob/3b79f38cb554809a45a0ccd6d9d6752b6ad948c2/src/SdCard/SdSpiCard.h#L122.
55. Greiman, William. “SdSpiCard.h.” Github, 2019, 54. https://github.com/greiman/SdFat/blob/3b79f38cb554809a45a0ccd6d9d6752b6ad948c2/src/SdCard/SdSpiCard.h#L207.
56. Greiman, William. “Why Is the SD Library Slow.” *Why Is the SD Library Slow?*, 2011, forum.arduino.cc/index.php?topic=49649.msg354701#msg354701.
57. Fennema, Jelte. “PyLaTeX.” *PyLaTeX - PyLatex 1.3.0 Documentation*, 1.3.0, 2015, jeltef.github.io/PyLaTeX/latest/.
58. Leng, Ting, et al. “Graphene Nanoflakes Printed Flexible Meandered-Line Dipole Antenna on Paper Substrate for Low-Cost RFID and Sensing Applications.” *IEEE Antennas and Wireless Propagation Letters*, vol. 15, 2016, pp. 1565–1568. *Institute of Electrical and Electronics Engineers (IEEE)*, doi:10.1109/lawp.2016.2518746.

59. Pogna, Eva A. A., et al. “Photo-Induced Bandgap Renormalization Governs the Ultrafast Response of Single-Layer MoS2.” *ACS Nano*, vol. 10, no. 1, 2016, pp. 1182–1188. *American Chemical Society (ACS)*, doi:10.1021/acsnano.5b06488.